CONTRAST MEDIA & MOLECULAR IMAGING

Received: 24 June 2012, Revised: 21 September 2012, Accepted: 28 September 2012, Published online in Wiley Online Library

(wileyonlinelibrary.com) DOI: 10.1002/cmmi.1514

Synthesis and *in vitro* evaluation of MR molecular imaging probes using J591 mAb-conjugated SPIONs for specific detection of prostate cancer

Mohammad Abdolahi[a], Daryoush Shahbazi-Gahrouei[a], Sophie Laurent[b], Corine Sermeus[b], Farzin Firozian[c], Barry J. Allen[d], Sebastien Boutry[b,e] and Robert N. Muller[b,e]*

Carcinoma of the prostate is the most frequent diagnosed malignant tumor in men and is the second leading cause of cancer-related death in this group. The cure rate of prostate cancer is highly dependent on the stage of disease at the diagnosis and early detection is key to designing effective treatment strategies. The objective of the present study is to make a specific MR imaging probe for targeted imaging of cancer cells. We take advantage of the fact that many types of prostate cancer cells express high levels of prostate-specific membrane antigen (PSMA) on their cell surface. The imaging strategy is to use superparamagnetic iron oxide nanoparticles (SPIONs), attached to an antibody (J591) that binds to the extracellular domain of PSMA, to specifically enhance the contrast of PSMA-expressing prostate cancer cells. Conjugation of mAb J591 to commercial SPIONs was achieved using a heterobifunctional linker, sulfo-SMCC. Two types of prostate cancer cell lines were chosen for experiments: LNCaP (PSMA+) and DU145 (PSMA−). MRI and cell uptake experiments demonstrated the high potential of the synthesized nanoprobe as a specific MRI contrast agent for detection of PSMA-expressing prostate cancer cells. Copyright © 2012 John Wiley & Sons, Ltd.

Keywords: prostate cancer; prostate specific membrane antigen (PSMA); superparamagnetic iron oxide nanoparticles; nanoprobe; magnetic resonance imaging

1. INTRODUCTION

Carcinoma of the prostate is the most frequently diagnosed malignant tumor in men and is the second leading cause of cancer-related death in this group (1). Despite the efficacy of local therapy (surgery or radiation therapy) for treating localized disease, the cure rate is highly dependent on the stage of disease at the diagnosis and early detection of prostate cancer is key to designing effective treatment strategies (2,3). However, in its early stages, prostate cancer (PC) rarely does have specific symptoms and the majority of men are diagnosed with advanced PC at the time of diagnosis (4,5). Advanced PCs often develop metastases and, once cancer has metastasized, even the best curative treatment can only prolong life with minimal hope of a cure (6–9).

Diagnosis of prostate cancer initially comes from a prostate-specific antigen (PSA) blood test as well as the digital rectal examination. Other modalities such as transrectal ultrasonography (TRUS) and magnetic resonance imaging (MRI) help the diagnosis of diseases (10,11). Determination of PSA is the mainstay of PC detection, and has led to a reduction in the incidence of metastasis over the last years (12). However, PSA is organ-specific and not disease-specific, so PC is not rare among men with normal-range PSA levels. There also remains growing concern regarding the potential risk of over-diagnosis and, consequently, overtreatment of potentially indolent disease (13–15).

TRUS is routinely used to perform prostate biopsies and brachytherapy seed placement. Unfortunately, PC can be isoechoic and indistinguishable from the surrounding normal prostate gland tissue, resulting in biopsies not specifically targeted to areas most likely to be malignant (16,17). Another modality in prostate cancer

* *Correspondence to: R. N. Muller, Department of General, Organic and Biomedical Chemistry, NMR and Molecular Imaging Laboratory, University of Mons, Mons, Belgium. Email: robert.muller@umons.ac.be*

a *M. Abdolahi, D. Shahbazi-Gahrouei*
Department of Medical Physics and Medical Engineering, School of Medicine, Isfahan University of Medical Sciences, Isfahan, Iran

b *S. Laurent, C. Sermeus, S. Boutry, R. N. Muller*
Department of General, Organic and Biomedical Chemistry, NMR and Molecular Imaging Laboratory, University of Mons, Mons, Belgium

c *F. Firozian*
Department of Pharmaceutics, School of Pharmacy and Pharmaceutical Sciences, Isfahan University of Medical Sciences, Isfahan, Iran

d *B. J. Allen*
Faculty of Medicine, University of New South Wales, Kogarah, NSW, 2217, Australia

e *S. Boutry, R. N. Muller*
Center for Microscopy and Molecular Imaging, Rue Adrienne Bolland 8, 6041 Charleroi, Belgium

diagnosis is the use of imaging techniques. A major goal for prostate cancer imaging is more accurate disease detection, localization, staging and local recurrence detection in patients (11). Currently, MRI, computed tomography (CT) scan and nuclear medicine are used for diagnosing, staging and monitoring of patients with PC; however, they lack enough sensitivity for early detection and provide limited information for disease staging (17–19). Among imaging techniques, MRI of the prostate can aid in many aspects of prostate cancer management, from initial detection to treatment planning and follow-up (20). The high spatial resolution of MR can be combined with specific MR molecular imaging agents to improve the specificity and sensitivity of cancer imaging. A promising strategy to improve the specificity and sensitivity of cancer imaging is to use biomarker target-specific imaging probes (21–23). These agents can accumulate at the site of the pathology, and provide sufficient and robust signal to enhance contrast from highly selected pathological tissues, which would otherwise be difficult to distinguish from surrounding normal tissue.

With regards to tumor markers in prostate cancer the most well established prostate-restricted cell surface antigen yet identified is prostate-specific membrane antigen (PSMA) (24–26). PSMA is a 100 kDa, cell surface type II membrane glycoprotein with folate hydrolase activity, which is highly expressed by all prostate cancers as well as by nonprostatic tumor neovasculature and the vascular endothelium of virtually all solid sarcoma and carcinoma tumors, without any expression on normal vascular endothelium (27,28). The cDNA sequence analysis and protein homology show that PSMA consists of 750 amino acids containing a proposed N-terminal 19 amino acids domain, 24 amino acids transmembrane domain and the remaining 707 amino acids domain (29,30). In viable cells the intracellular site is masked by the intact cell membrane and is 'invisible' to circulating anti-PSMA antibodies (Abs). Therefore, for targeted of viable cells it is very important to use an anti-PSMA agent that can detect extracellular domain of PSMA (24,31). Several anti-PSMA Abs have been developed recently that bind the extracellular PSMA domain (32,33). The anti-PSMA antibody, J591, used in this research can detect two distinct noncompeting extracellular epitopes of PSMA (PSMAext1 and PSMAext2) and so is capable of binding viable PSMA expressing cells (33,34). Subsequent *in vitro* and *in vivo* studies proposed J591 as a most promising candidate for targeted diagnosis and therapy of viable prostate cancer cells (31,35,36). This work describes the production and evaluation of magnetic nanoprobe (superparamagnetic iron oxide, SPIO–J591) for targeted MR imaging of PSMA-expressing prostate cancer cells.

2. MATERIAL AND METHODS

2.1. Materials

Sulfo-SMCC crosslinker [sulfosuccinimidyl-4-(*N*-maleimidomethyl) cyclohexane-1-carboxylate], Traut's Reagent (2-iminothiolane) and cysteine were purchased from Sigma Aldrich (Bornem, Belgium). Amino group-functionalized polyethylene glycol (PEG)-coated superparamagnetic iron oxide nanoparticles (20 nm; nanomag®-D-spio) were gifted by Micromode Company (Micromod Partikeltechnologie GmbH, Rostock, Germany). A MACS separator with MS columns was purchased from Miltenyi Biotec GmbH (Gladbach, Germany). All other chemicals were supplied by Sigma Aldrich and used as received. J591 monoclonal antibody was obtained from Professor Neil H. Bander (Cornell University, New York, USA). Cell culture media and fetal bovine sera (FBS) were obtained from GIBCO, Invitrogen Corporation (Carlsbad, CA, USA). Prostate cancer cell lines, PC3 and LNCaP, were purchased from Cell Lines Service (CLS, Eppelheim, Germany).

2.2. Conjugation of J591 Antibody with Nanoparticles

The SPIO–J591 nanoprobes were synthesized following a three-step process. The first step was the modification of Ab primary amines with iminothiolane to introduce sulfhydryl groups into the antibody (Fig. 1A). Typically, 8 μl of 7 mM Trauts reagent solution were added to 400 μl of pure antibody solution in phosphate buffered saline (PBS)/2mM EDTA (ethylenediaminetetraacetic acid)

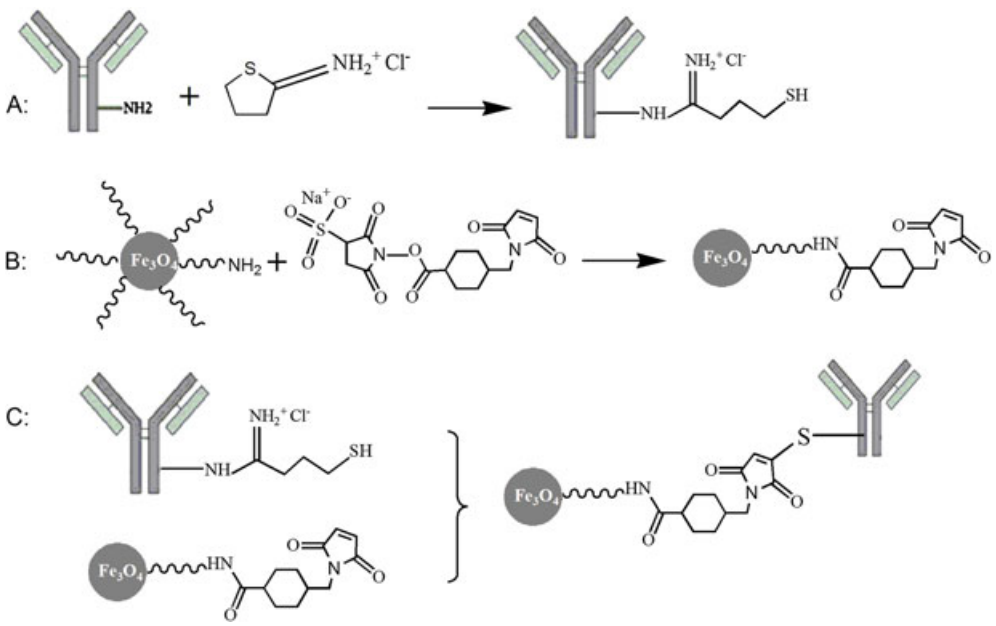

Figure 1. Conjugation of SPIONs to J591 antibody. (A) Functionalization of SPIO-PEG-NH2 with Sulfo-SMCC. (B) functionalization of antibody with SH groups using Traut's reagent. (C) Conjugation of antibody to SPIO.

buffer and stirred for 1 h at room temperature. To remove unconjugated iminothiolane, the solution was washed three times using 10 kDa cutoff Amicon centrifugal filter units (Millipore) with PBS as an eluent. The sulfhydryl groups of antibody react with the maleimide groups at the surface of sulfo-SMCC activated SPIO.

In a second step, superparamagnetic iron oxide nanoparticles (SPIONs) were modified with sulfo-SMCC to introduce maleimide groups (Fig. 1B). Briefly, 100 µl of 14.35 µM Sulfo-SMCC solution in dimethyl sulfoxide (DMSO) was added to 5 mg of nanoparticles in PBS–EDTA buffer and stirred for 1 h at room temperature. To remove unreacted sulfo-SMCC, the solution was washed with PBS–EDTA buffer with size exclusion columns (PD-10, GE Healthcare Life Sciences).

In the last step, conjugation (Fig. 1C) was achieved by addition of the maleimide particle suspension to the SH-labeled antibody and incubation on a rotating shaker for 3 h at room temperature. Remaining functional groups were blocked by addition of 100 µl of 20 mM freshly prepared cystein solution. Finally the unconjugated antibodies were separated from antibodies labeled particles by magnetic columns in a high gradient magnetic field system (MACS separator).

2.3. Characterization

The particle size distribution of nanomag®-D-spio and J591–SPIO were measured by photon correlation spectroscopy (PCS) using a Zetasizer ZS (Malvern Instruments, Worcestershire, UK) directly after mechanical shaking. Sample morphology was examined by transmission electron microscopy (Tecnai 10 (80 kV), FEI Company, USA).

To study the magnetic properties of synthesized nanoprobe, the nuclear magnetic resonance dispersion (NMRD) profiles were recorded with a field cycling relaxometer (Spinmaster FFC2000, STELAR, Italy) measuring the longitudinal relaxation rates (R_1) at 310 K in a field range extending from 0.01 to 50 MHz of proton Larmor frequency. Additional measurements of relaxation rate ($R_{1,\,2}$) were performed at 20 and 60 MHz and 310 K on a Bruker Minispec system mq-20 and mq-60 (Bruker, Karlsruhe, Germany) according to the inverse recovery sequence and the Carr–Purcell–Meiboom–Gill sequence, respectively.

2.4. Total iron and Antibody Concentration

The binding of antibody molecules to SPIO and the amount of immobilized antibody were confirmed by the Bradford assay method as well as the measurements of the hydrodynamic size. Forty microliters of Coomassie Plus reagent concentrate (Bio-Rad, USA) were added to 160 µl of dispersion of nanoparticles, either mAb-coated or noncoated, and after 10 min of incubation, the absorbance was measured at 595 nm using a microplate reader (Stat Fax, Awareness Technologies, USA). The results were compared with a standard curve of BSA solution in the concentration ranging from 10 to 150 µg ml^{-1}.

The iron concentration of samples was determined by relaxometry measurements at 20 MHz after digestion using a microwave oven. This was achieved by mineralization of sample in acidic conditions (0.2 ml sample, 0.6 ml HNO_3 and 0.3 ml H_2O_2) using a microwave oven (Milestone MLS-1200, Sorisole, Italy). The millimolar iron concentration was estimated from the R_1 relaxation rate of samples, using equation (1):

$$[\mathrm{Fe}] = \frac{\left(R_1^{\mathrm{obs}} - R_1^{\mathrm{dia}}\right)}{r_1\left(s^{-1}\mathrm{mM}^{-1}\right)}$$

where R_1^{obs} is the observed longitudinal proton relaxation rate, R_1^{dia} is the relaxation rate of water protons in the absence of the contrast agent, and r_1 is the longitudinal relaxivity defined as the increase of the water proton relaxation rates induced by 1 mmol per liter of paramagnetic center. R_1^{obs} is the relaxation rate which is measured in the solution containing the sample; R_1^{dia} and r_1 were obtained from a standard curve built by measuring the R_1 of various dilutions of the mineralized standard sample of iron (ICP standard; Sigma Aldrich; Fig. 3).

2.5. Cell Culture

LNCaP, a PSMA-expressing (PSMA+) and DU145, a PSMA negative (PSMA−) adherent human prostate cancer cell lines were obtained from Cell Lines Service (CLS, Eppelheim, Germany). Cells were grown in Dulbecco's modified Eagle medium supplemented with 2 mM L-glutamine, 1% nonessential amino acid (NEAA), 1 mM sodium pyruvate, 10% fetal bovine serum and 1% penicillin–streptomycin (Gibco, Grand Island, NY, USA) except that 1.5 g l^{-1} sodium bicarbonate and 0.1 mM nonessential amino acids was used for DU145. The cells were grown in 250 ml flasks, at 37 °C in a humidified atmosphere with 5% CO_2. For subculture and harvesting of the cells, they were washed with PBS and subsequently treated with 3 ml TrypLE (Gibco, Grand Island, NY, USA) for 3 min to detach the cells. About 10 ml of culture medium was added to neutralize the TrypLE. The cells were then centrifuged at 3000 rpm for 10 min to remove medium, resuspended in complete media and reseeded into new culture flasks.

2.6. Flow Cytometry

To detect cell-surface expression of PSMA on the LNCaP and DU145 cell lines, indirect immunofluorescence staining was performed. In brief, cells were trypsinized and washed with PBS containing 0.1% fetal bovine serum (FBS), and 10^6 cells per tube from each cell line were transferred into facs tubes. The cells were resuspended in 90 µl of washing buffer and were preblocked with FcR Block (human) reagent (Miltenyi) for 10 min at room temperature in the dark. After blocking, primary J591 anti PSMA antibody (1:150 dilution) was added to each cell tube (one tube of each cell line as a control), incubated for 30 min in the dark at room temperature, and then washed 3 × 5 min using a washing buffer. After washing, the cells were resuspended and incubated in goat anti-mouse FITC monoclonal antibody for an additional 30 min at room temperature in the dark. Cells were then washed, resuspended in 0.5 ml of PBS plus 0.1% FBS and analyzed immediately using a using a CyAN-ADP flow cytometer (Beckman Coulter).

2.7. *In Vitro* Cytotoxicity

Nanomag®-D-spio and synthesized nanoprobe cytotoxicity against LNCaP and DU145 cells were evaluated by using the 3-(4,5-dimethylthiazol-2-yl)-2,5diphenyltetrazolium bromide (MTT) assay (Sigma–Aldrich) (40). Exponentially growing LNCaP and DU145 cells were seeded at a density of 2×10^4 cells per well in 96-well plates (Cell Star, Germany). The plates were incubated for 24 h in a humidified incubator with a CO_2 concentration of 5% to allow

adherence of the cells. Once adhered, the cells were incubated with either 0.1 ml of medium containing nanomag®-D-spio and SPIO–J591 at iron concentrations ranging from 0.15 to 2.4 mM for 2, 8 and 24 h. The culture medium without any particle was used as the control.

After the incubation time, 10 µl per well (5 mg ml^{-1}) MTT was added and incubation was continued for a further 3 h. The medium was carefully removed and the formazan crystals (indicating cell viability) were solubilized by adding 100 µl DMSO (Sigma–Aldrich) per well. The absorbance was determined at 570 nm by the Statfax-microplate reader (Awareness Technology, USA). Experiments were performed in triplicate and cell survival was determined as a percentage of viable cells in comparison with control wells. One-way one-way analysis of variance (ANOVA) and correlation coefficient between viability and iron concentration were used to determine whether the SPIONs caused any significant cytotoxicity.

2.8. Cellular SPION Uptake Studies

To measure the iron uptake, human prostate cancer LNCaP and DU145 cells were detached and washed three times with PBS and approximately 4×10^6 cell per tube of each cells were suspended in 15 ml tube and incubated with culture medium containing nanomag®-D-spio or SPIO–J591 at Fe concentrations of 3 mM (one tube control) for 2 h at room temperature.

After incubation, cells were washed with PBS three times and mineralized in 0.5 ml of 5 M HCl for 3 h in a water bath at 80 °C. Iron concentration in mineralized cell samples was determined by measuring the longitudinal relaxation rate (R_1) at 310 K and 1.4 T (60 MHz) on a Bruker Minispec mq60 as described above. The SPION uptake per cell was calculated following equation (1). The results were compared to a standard curve of iron concentration obtained by measuring the R_1 of various dilutions of mineralized standard sample of iron at 310 K and 1.4 T (60 MHz) on a Bruker Minispec mq60.

2.9. Prussian Blue Staining

The specificity and cellular uptake of J591 functionalized and nonfunctionalized SPIONs to the LNCaP and DU145 cells were examined by Prussian blue staining. Briefly, cells were seeded at a density of 2×10^5 cells per well, in 12-well plates (Cell Star, Germany) then cells were incubated overnight at 37 °C in a humidified incubator with a CO_2 concentration of 5%, to allow adherence of the cells incubated for 24 h. Following adherence the cell medium was removed and then cells washed with PBS and continued incubation with 1 ml of the culture media containing 2 mM Fe concentration of each particle for 2 h at room temperature. Following incubation cells were washed in PBS and fixed in 4% paraformaldehyde for 20 min. Cells were then washed with PBS (3×), and stained using Prussian blue solution comprising equal volumes of 2% hydrochloric acid aqueous solution and 2% potassium ferrocyanide (II) trihydrate. The stained plate images were acquired with a Leica fluorescent microscope (Leica DM5500 B, Chicago, IL, USA).

2.10. Magnetic Resonance Imaging

The potential of J591–SPIO conjugates for MRI was investigated *in vitro* after incubation with LNCaP or DU145 cells. In brief, approximately 4×10^6 cell per tube of each cell lines were suspended in a 15 ml tube and incubated with fresh culture medium containing media alone (as a control), nonfunctionalized SPIO or J591–SPIO at Fe concentrations of five different doses (5, 10, 20, 40, 80 µg ml^{-1}) for 2 h at room temperature. After incubation, cells were washed with PBS three times and fixed with ice-cold 4% paraformaldehyde in PBS for 20 min. Following fixation the cells were washed in PBS and resuspended in 1 ml 2% agar gel in a special glass NMR tube.

The samples were then scanned and T_2-weighted images were acquired with a spin-echo imaging sequence using a 7 T horizontal bore small animal MR Scanner imaging system (Bruker Biospec, Germany). Imaging parameters were as follows: repetition time, 2500 ms; echo time, 33 ms; field of view, 250 × 250 mm; matrix size, 256 × 256; slice thickness, 3 mm. The data from regions of interest were drawn to consistently measure mean signal intensity at the identical position within each phantom vial.

3. RESULTS AND DISCUSSION

3.1. Synthesis

The overall aim of the work in this research was to generate antibody targeted SPION conjugates for targeted imaging of prostate cancer. The J591 monoclonal antibody was conjugated to SPIONs via iminothiolane/SMCC coupling method (Fig. 1). The primary amines of antibody were nonselectively modified with Trauts reagent to introduce sulfhydryl groups to the antibody. The sulfhydryl groups of antibody reacted with the maleimide groups at the surface of sulfo-SMCC activated SPIONs. The feasibility of successfully grafting antibody molecules to SPIONs was confirmed by Bradford assay method as well as the measurements of the hydrodynamic size and shape of SPIONs using PCS and Transmission electron microscopy (TEM). Analyses by Bradford protein assay and spectrophotometric readings showed that the amount of immobilized antibody was 36 ± 4 µg Ab ml^{-1} of synthesized nanoprobe (Fig. 2). Thanks to a standard curve established with commercially available iron solution (ICP standard; Sigma Aldrich), the iron concentration of particles was estimated to be 43.88 and 24.22 mM for nanomag®-D-spio and J591–SPIO respectively by MR relaxometry method (Fig. 3).

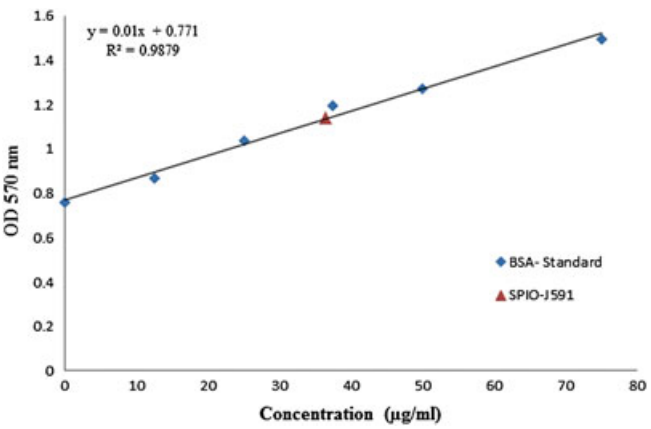

Figure 2. Antibody concentration measurement by Bradford Assay. Standard curve of BSA concentration (µg/mL) versus absorbance (at 595 nm) was used to determine the antibody concentration of synthesized nanoprobe.

3.2. Characterization

The particle size distribution before and after antibody conjugation was determined by PCS. Figure 4 shows the hydrodynamic particle diameter of nanomag®-D-spio and J591–SPIO. Hydrodynamic diameters were determined to be 18.65 ± 0.21 nm for nanomag®-D-spio and 24.68 ± 0.22 nm for J591–SPIO. Figure 5 (a and b) shows TEM images for plain and antibody conjugated SPIO, respectively. Spherical-shaped, average particle size calculated from TEM was 10–20 nm for both nanomag®-D-spio and J591–SPIO. The morphology study of particles from TEM image suggests that antibody molecules conjugated to SPIONs reduce the agglomeration of nanomag®-D-spio particles.

NMRD profiles (Spinmaster FFC2000, STELAR, Italy) were used to examine the magnetic properties of nanomag®-D-spio and J591–SPIO from 0.01 to 50 MHz of proton Larmor frequency. It can be observed from Fig. 6 that the magnetic properties of the SPIONs did not change significantly when conjugated to antibody. The fitting of the NMRD profiles by a theoretical relaxation model (37,38) [equation (2)] allowed the determination of the crystal radius (r) and the specific magnetization (M_{sat}; Table 1).

$$R_1 = \frac{32\pi}{135000}\mu^2\gamma^2\frac{N_a C}{rD}\left[7P\frac{L(X)}{X}J_F(\omega_S,\tau_D,\tau_N) + \left[7(1-P)\frac{L(X)}{X} + 3\left(1 - 2\frac{L(X)}{X} + L^2(X)\right)\right]J_F(\omega_I,\tau_D,\tau_N) + 3L^2(X)J_A(\omega_I,\tau_D)\right]$$

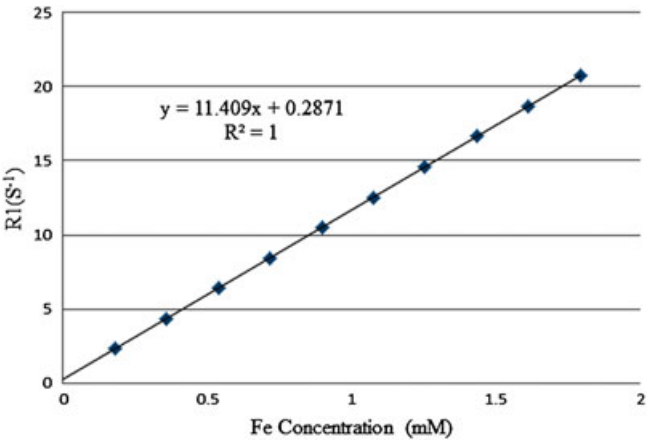

Figure 3. Calibration curve of Iron concentration vs relaxation rate at 20 MHz. The millimolar iron concentration was estimated from the R_1 relaxation rate of samples, using equation 1; Where R_1^{dia} is the diamagnetic longitudinal proton relaxation rate, i.e. the relaxation rate of water protons in the absence of the contrast agent, and r_1 is the slope of the calibration curve.

R_1 and R_2 relaxation rate measurements of particles were performed on a Bruker Minispec operating at 20 and 60 MHz. A summary of the longitudinal and transversal relaxivity is provided in Table 1.

3.3. *In Vitro* Cytotoxicity

For each nanoprobe to be suitable as a targeted MRI contrast agent, they should show minimal toxicity to the targeted cell. The *in vitro* cytotoxic effect of nonfunctionalized SPIONs and J591–SPIO was assessed using the standard MTT assay, using LNCaP and DU145 cell lines. The results after different time incubation with different concentration of iron for both cell lines showed >80% cell viability in relation to the control sample, in most cases (Fig. 7). The statistical analysis by ANOVA followed by Duncan, multiple range test showed statistically significant evidence of nonfunctionalized or functionalized SPIO toxicity to cells (p-value = 0.02). The p-values for 2–8, 2–24 and 8–24 h incubation of DU145 cell line with SPIO–J591 and nanomag®-D-spio was 0.007–0.015, 0.03–0.003 and 0.04–0.36, respectively. In comparison to the LNCaP cell line, these values were 0.17–0.21,

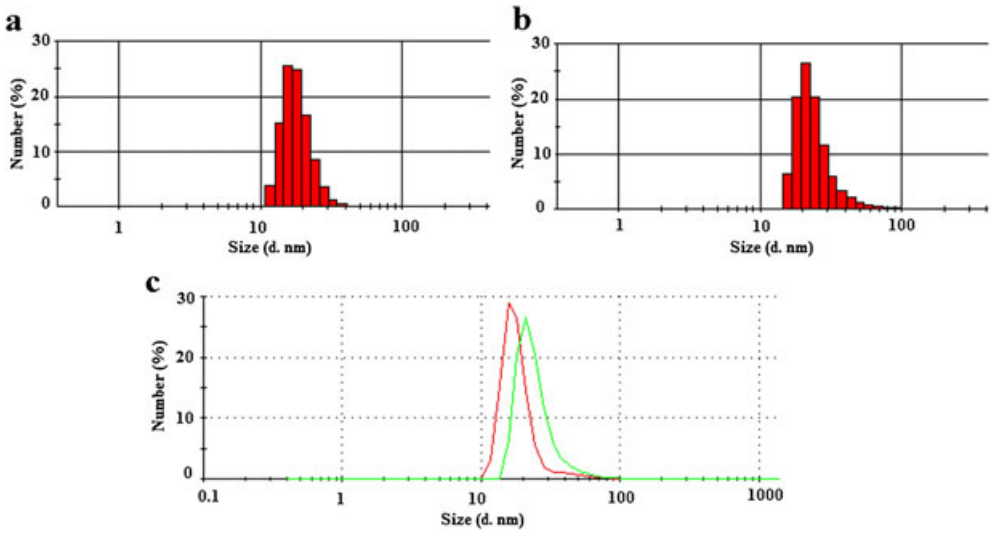

Figure 4. Hydrodynamic diameter of a) nanomag-D-SPIO(18.65 nm) and b) J591-SPIO NPs (24.68 nm).

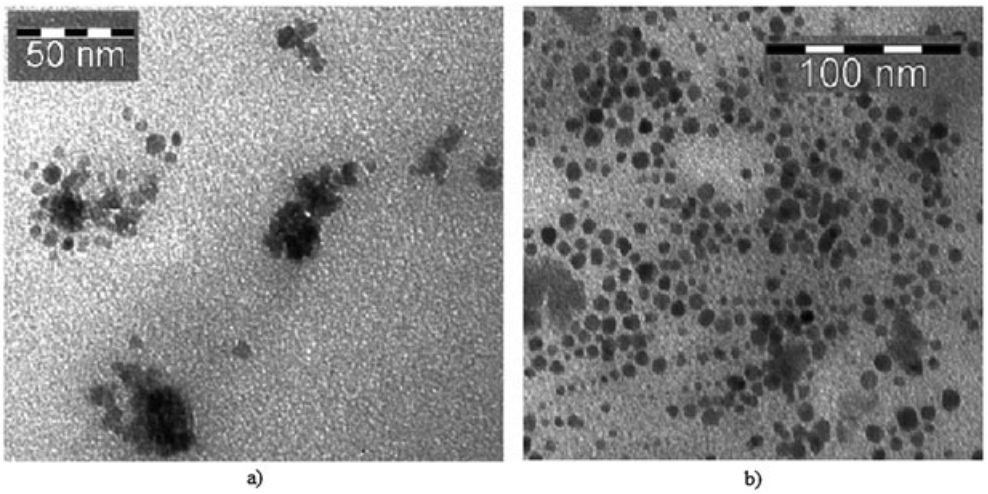

Figure 5. TEM images for plain and antibody conjugated SPIO a) nanomag-D-SPIO, b) J591-SPIO, antibody binding causes a significant reduction of particle agglomeration. The average particle size of particles estimated from TEM images was about 10–20 nm.

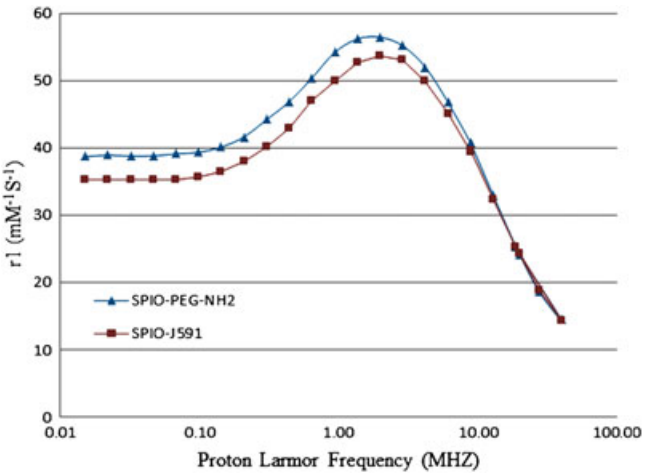

Figure 6. NMRD profiles of Nanomag-D-SPIO and synthesized nanoprobes.

0.15–0.02 and 0.48–0.02. As can be seen, the *p*-values were insignificant for most of LNCaP cell line compared with the DU145 cells.

The results of MTT assay show a moderate negative correlation [$r = (-0.16)$–(-0.71)] between concentration and viability for most assays after 2 and 8 h incubation, but when taking 24 h incubation into account, a positive correlation ($r = 0.08$–0.73) between the concentration and viability was found.

3.4. Flow Cytometry

For targeted imaging, identifying an antigen that is uniquely expressed or overexpressed on tumor cells is of crucial importance. Flow cytometric analysis was performed to confirm the availability of the desired PSMA antigen on the cell surface. Indirect immunofluorescent staining of LNCaP and DU145 cell lines showed that LNCaP cells express high levels of PSMA on their cell surface (95 %), whereas DU145 cells lack PSMA expression (2–3%) (Fig. 8). These results are in agreement with previously published studies (31,39).

3.5. Cellular SPION Uptake Studies

To determine the ability of functionalized SPIONs to target positive PSMA prostate cancer cells, we compared the cell uptake efficiency of J591–SPIO nanoparticles between LNCaP (positive) and DU145 (negative) cells. Changes in T_1 and T_2 parameters which are due to the incubation of synthesized nanoprobe and nanomag®-D-spio with cell lines are illustrated in Table 2. Also, iron concentration measurement of cells after incubation with particles showed considerably increased Fe uptake in positive LNCaP cells over negative DU145 cells (Fig. 9). The intracellular Fe concentration for LNCaP cells after incubation with J591–SPIO and nanomag®-D-spio was 1.45 and 0.33 mM, respectively. In comparison, these values were 0.23 and 0.30 mM, respectively, for a DU145 cell line.

Table 1. Longitudinal and transversal relaxivities (r_1 and $r_{2)}$ of nanomag®-D-spio and synthesized nanoprobe at 20 and 60 MHz at 37 °C (Minispec) and the saturation magnetization and size of particles estimated by nuclear magnetic resonance dispersion profile data. The results are from three independent experiments ($n = 3$)

Particle	r_1 (s^{-1} mM^{-1})		r_2 (s^{-1} mM^{-1})		r_2/r_1		M_{sat} (A m^2 kg^{-1})	r (nm)
	20 MHz	60 MHz	20 MHz	60 MHz	20 MHz	60 MHz		
SPIO–PEG–NH_2	21.8 ± 0.42	8.3 ± 0.1	126.8 ± 1.4	137.2 ± 2.1	5.8 ± 0.04	16.5 ± 0.05	37.7	8.48
SPIO–J591	21.8 ± 0.23	7.7 ± 0.08	112 ± 0.86	119.8 ± 1	5.1 ± 0.01	15.5 ± 0.03	37.7	8.33

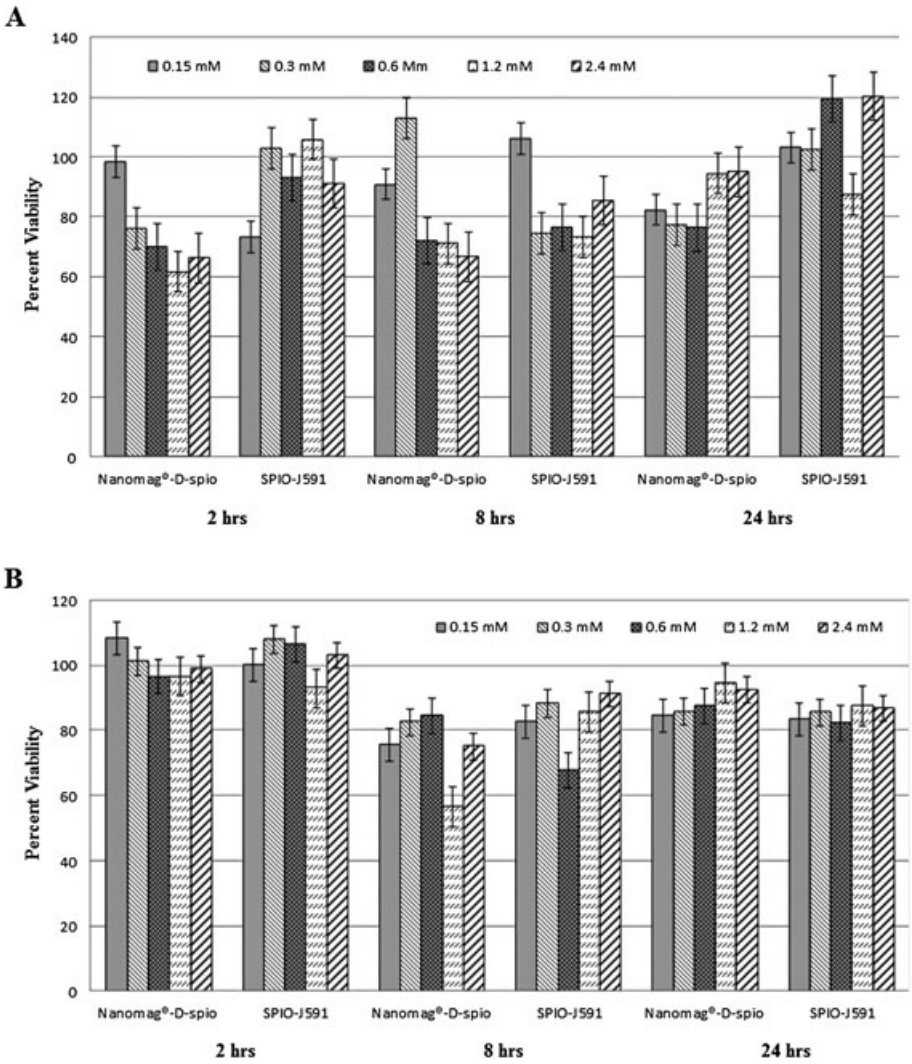

Figure 7. In vitro assessment of the cytotoxicity of Nanomag®-D-spio and SPIO-J591 to LNCaP (A) and DU145 (B) prostate cancer cell lines by the MTT assay. The cells were incubated with Nanomag®-D-spio or SPIOJ591 at equivalent iron concentrations ranging from 0.15 to 2.4 mM for 2, 8 and 24 h. The cytotoxicity was evaluated by the MTT assay.

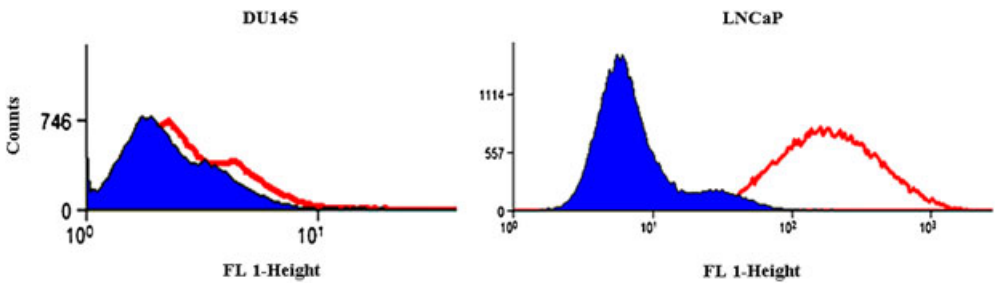

Figure 8. Flowcytometry test shows LNCaP cells express high levels of prostate-specific membrane antigen (PSMA) on their cell surface (right) whereas DU145 cells lack PSMA expression (left).

Targeting specificity to the positive PSMA prostate cancer cells of J591–SPIO was also confirmed with Prussian blue staining. Blue areas or spots (Fig. 10) represented the targeting effect and SPIO uptake of functionalized particles on the cellular uptake behavior. There was no blue color appearance in the cells incubated with nonfunctionalized SPIO or PSMA negative (DU145) cells.

3.6. Magnetic Resonance Imaging

The ability of the synthesized nanoprobe to targeting specifically to the PSMA positive cells was also confirmed with MR imaging techniques. The results displayed in Fig. 11 demonstrate that nanoparticles functionalized with J591 monoclonal antibody

Table 2. Relaxation rate of LNCaP and DU145 cell lines after incubation with nanomag®-D-spio and synthesized nanoprobe at a frequency of 60 MHz. The results are from three independent experiments ($n = 3$)

Relaxation (s^{-1})	DU145 (PSMA−)		LNCaP (PSMA$^+$)	
R_1	0.42 ± 0.02		0.52 ± 0.01	
R_2	0.60 ± 0.008		0.89 ± 0.01	
	SPIO–J591	*nanomag®-D-spio*	*SPIO–J591*	*nanomag®-D-spio*
R_1	0.65 ± 0.01	1.47 ± 0.05	7.28 ± 0.08	1.97 ± 0.02
R_2	0.79 ± 0.01	1.82 ± 0.03	9.67 ± 0.13	2.60 ± 0.06

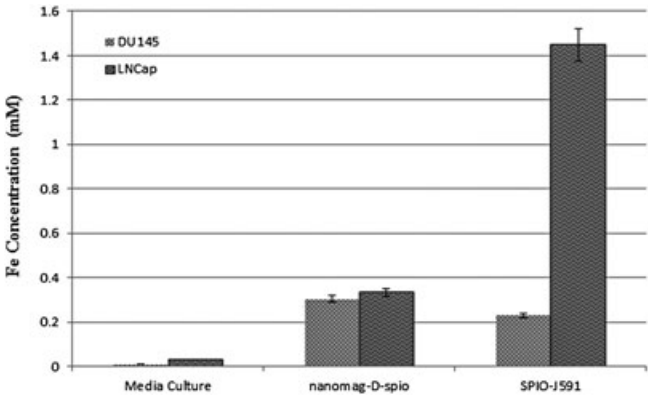

Figure 9. Iron uptake of cells after incubation of 4×10^6 cells from each cell line with nanomag®-D-spio and J591-SPIO at iron concentration of 3 mM at room temperature for 2 hours.

reduced by 95% MR image intensity in LNCaP cell line compared with the 14% reduction in DU145 cell lines in an Fe concentration of 80 μg ml^{-1}. Signal intensity reduction induced by nontargeted SPIONs was 48 and 40% in LNCaP and DU145 cell lines, respectively. However, there was about 30% more reduction in signal intensity for the DU145 cells with nontargeted SPIONs, which strongly suggests the effectiveness of the $-NH_2$ functional group in nonspecific uptake by this cell line, compared with particles whose amine groups were shielded by conjugated antibodies.

Differences between the signal intensities were statistically tested using ANOVA followed by Duncan, multiple range test. The analysis showed statistically significant signal intensity difference between nonfunctionalized or functionalized SPIO at same Fe concentration for both DU145 and LNCaP cells (p-value < 0.02).

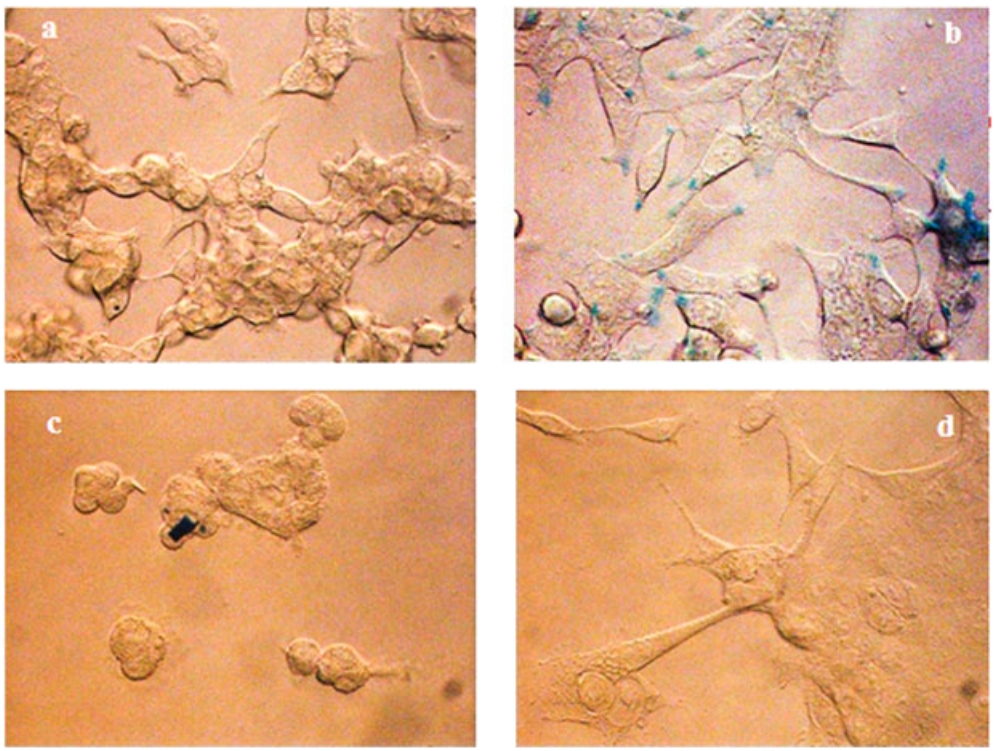

Figure 10. Prussian blue staining images(×40) of a) LNCaP cells (105) after 2 h incubation with Nanomag®-D-spio, b) SPIO-J591 nanoprobe, c) Prussian blue staining images of DU145 cells after 2 h incubation with Nanomag®-D-spio and d) SPIO-J591 nanoprobe. Fe concentration was 2 mM in all tests and after incubation cells treated with Prussian blue solution for 30 min.

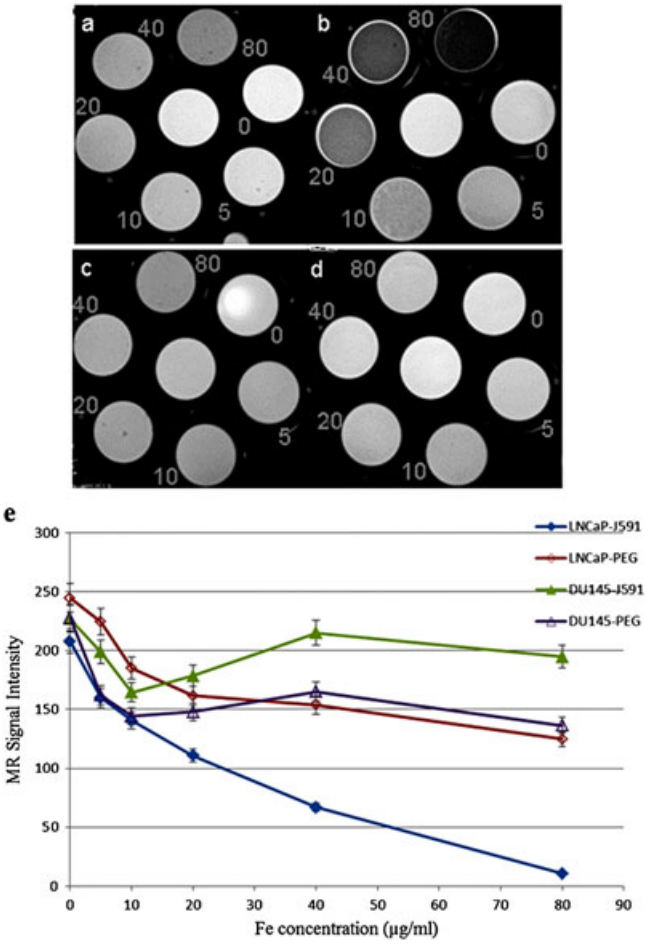

Figure 11. T2-weighted imaging of LNCaP cells (3×10^6) after 2 h incubation with Nanomag®-D-spio (a) and SPIO-J591 nanoprobe (b) and DU145 cells after incubation with Nanomag®-D-spio (c) and SPIO-J591 nanoprobe (d) at Fe concentration of 0, 5, 10, 20, 40, 80 µg/ml.(The vial in the middle is PBS alone without any contrast agent) (e) Shows the MR signal intensity.

4. CONCLUSIONS

Early detection of prostate cancer is key to designing effective treatment strategies. For early and more accurate and specific disease characterization, we used molecular magnetic resonance imaging technique, through the synthesis of targeted magnetic nanoprobes. The novel agent used in the study was prepared with a monoclonal antibody J591conjugated to SPIOs to target the PSMA receptor expressed by most of prostate tumor cells.

Previous studies with radiolabeled J591 mAb showed high tumor targeting, low nonspecific organ uptake, nonimmunogenicity, nontoxicity and the capability to target PC metastases with high sensitivity and specificity (35,41).

Results of this study showed that, through functionalization of SPIONs by J591, monoclonal antibody specific binding of the SPIONs to the PSMA-expressing cells is achievable *in vitro*. The results of Prussian blue staining and measurement of iron uptake by cells showed high targeting and specificity of J591–SPIO to PSMA-positive prostate cancer cells. In addition, *in vitro* MRI imaging of prostate cancer cells demonstrated that J591-conjugated SPIO with high stability and sensitivity have potential to be used as an MR contrast agent for the detection of PSMA-positive prostate cancer cells.

With development of this and similar imaging specific vehicles, more effective and detailed diagnosis of prostate cancer through high concentrations of SPIONs at the tumors site is achievable and, because of high cell uptake of SPIONs, it could be used for more effective hyperthermia to treat the disease (42,43).

Acknowledgements

The author thanks Dr Cordula Gruettner (micromod Particle technology GmbH, Rostock, Germany) and for kindly providing SPIO particles and her discussion and meticulous guidance during this work. The authors also thank Dr Lhomme Frederic (IMI, Institut d'Immunologie Médicale, Université Libre de Bruxelles, Brussels, Belgium) for his help in flow cytometry. This work was financially supported by Isfahan University of medical science (Grant-in-Aid for Scientific Research, no. 19550157), ARC (research contract AUWB-2010-10/15-UMONS-5), FNRS and ENCITE programs and it was performed in the framework of COST TD1004 and CM1006. The authors thank the Center for Microscopy and Molecular Imaging (supported by the European Regional Development Fund and the Walloon Region) for their support.

REFERENCES

1. Jemal A, Siegel R, Xu J, Ward E. Cancer statistics, 2010. CA Cancer J Clin 2010;60(5):277–300; epub 2010/07/09.
2. Kelly KA, Setlur SR, Ross R, Anbazhagan R, Waterman P, Rubin MA, et al. Detection of early prostate cancer using a hepsin-targeted imaging agent. Cancer Res 2008;68(7):2286–2291; epub 2008/04/03.
3. Emonds KM, Swinnen JV, Mortelmans L, Mottaghy FM. Molecular imaging of prostate cancer. Methods 2009;48(2):193–199; epub 2009/04/14.
4. Lee CM, Jeong HJ, Cheong SJ, Kim EM, Kim DW, Lim ST, et al. Prostate cancer-targeted imaging using magnetofluorescent polymeric nanoparticles functionalized with bombesin. Pharm Res 2010;27(4):712–721; epub 2010/02/26.
5. Candas B, Cusan L, Gomez JL, Diamond P, Suburu RE, Levesque J, et al. Evaluation of prostatic specific antigen and digital rectal examination as screening tests for prostate cancer. Prostate 2000;45(1):19–35; epub 2000/08/29.
6. Bennett CL, Tosteson TD, Schmitt B, Weinberg PD, Ernstoff MS, Ross SD. Maximum androgen-blockade with medical or surgical castration in advanced prostate cancer: a meta-analysis of nine published randomized controlled trials and 4128 patients using flutamide. Prostate Cancer Prostatic Dis 1999;2(1):4–8; epub 2002/12/24.
7. Caubet JF, Tosteson TD, Dong EW, Naylon EM, Whiting GW, Ernstoff MS, et al. Maximum androgen blockade in advanced prostate cancer: a meta-analysis of published randomized controlled trials using nonsteroidal antiandrogens. Urology 1997;49(1):71–78; epub 1997/01/01.
8. Tannock IF, de Wit R, Berry WR, Horti J, Pluzanska A, Chi KN, et al. Docetaxel plus prednisone or mitoxantrone plus prednisone for advanced prostate cancer. New Engl J Med 2004;351(15):1502–1512; epub 2004/10/08.
9. Li Y, Cozzi PJ, Russell PJ. Promising tumor-associated antigens for future prostate cancer therapy. Med Res Rev 2010;30(1):67–101; epub 2009/06/19.
10. Ravizzini G, Turkbey B, Kurdziel K, Choyke PL. New horizons in prostate cancer imaging. Eur J Radiol 2009;70(2):212–226; epub 2008/11/11.
11. Futterer JJ, Heijmink SW, Spermon JR. Imaging the male reproductive tract: current trends and future directions. Radiol Clin N Am 2008;46(1):133–147, vii; epub 2008/03/11.
12. Garin JA, Mas AG. Metodos diagnosticos de la diseminacion prostatica. [The diagnosis of prostate cancer dissemination.] Arch Esp Urol 2006;59(10):1011–1020; epub 2007/02/08.
13. Schroder FH, Hugosson J, Roobol MJ, Tammela TL, Ciatto S, Nelen V, et al. Screening and prostate-cancer mortality in a randomized

European study. New Engl J Med 2009;360(13):1320–1328; epub 2009/03/20.
14. Thompson IM, Pauler DK, Goodman PJ, Tangen CM, Lucia MS, Parnes HL, et al. Prevalence of prostate cancer among men with a prostate-specific antigen level < or =4.0 ng per milliliter. New Engl J Med 2004;350(22):2239–2246; epub 2004/05/28.
15. Steuber T, Helo P, Lilja H. Circulating biomarkers for prostate cancer. World J Urol 2007;25(2):111–119; epub 2007/03/09.
16. Kelloff GJ, Choyke P, Coffey DS. Challenges in clinical prostate cancer: role of imaging. AJR Am J Roentgenol 2009;192(6):1455–1470; epub 2009/05/22.
17. Karam JA, Mason RP, Koeneman KS, Antich PP, Benaim EA, Hsieh JT. Molecular imaging in prostate cancer. J Cell Biochem 2003;90 (3):473–483; epub 2003/10/03.
18. DeGrado TR, Coleman RE, Wang S, Baldwin SW, Orr MD, Robertson CN, et al. Synthesis and evaluation of 18F-labeled choline as an oncologic tracer for positron emission tomography: initial findings in prostate cancer. Cancer Res 2001;61(1):110–117; epub 2001/02/24.
19. Kwee SA, Wei H, Sesterhenn I, Yun D, Coel MN. Localization of primary prostate cancer with dual-phase 18F-fluorocholine PET. J Nucl Med 2006;47(2):262–269; epub 2006/02/04.
20. Mazaheri Y, Shukla-Dave A, Muellner A, Hricak H. MRI of the prostate: clinical relevance and emerging applications. J Magn Reson Imaging 2011;33(2):258–274; epub 2011/01/29.
21. Weissleder R. Molecular imaging in cancer. Science 2006;312 (5777):1168–1171; epub 2006/05/27.
22. Massoud TF, Gambhir SS. Molecular imaging in living subjects: seeing fundamental biological processes in a new light. Gene Dev 2003;17(5):545–580; epub 2003/03/12.
23. Artemov D, Mori N, Ravi R, Bhujwalla ZM. Magnetic resonance molecular imaging of the HER-2/neu receptor. Cancer Res 2003;63 (11):2723–2727; epub 2003/06/05.
24. Bander NH, Trabulsi EJ, Kostakoglu L, Yao D, Vallabhajosula S, Smith-Jones P, et al. Targeting metastatic prostate cancer with radiolabeled monoclonal antibody J591 to the extracellular domain of prostate specific membrane antigen. J Urol 2003;170(5):1717–1721.
25. Sokoloff RL, Norton KC, Gasior CL, Marker KM, Grauer LS. A dual-monoclonal sandwich assay for prostate-specific membrane antigen: levels in tissues, seminal fluid and urine. Prostate 2000;43(2):150–157.
26. Wright GL, Jr, Haley C, Beckett ML, Schellhammer PF. Expression of prostate-specific membrane antigen in normal, benign, and malignant prostate tissues. Urol Oncol 1995;1(1):18–28; epub 1995/01/01.
27. Patri AK, Myc A, Beals J, Thomas TP, Bander NH, Baker JR, Jr. Synthesis and in vitro testing of J591 antibody–dendrimer conjugates for targeted prostate cancer therapy. Bioconjug Chem 2004;15 (6):1174–1181; epub 2004/11/18.
28. Chang SS, Reuter VE, Heston WD, Bander NH, Grauer LS, Gaudin PB. Five different anti-prostate-specific membrane antigen (PSMA) antibodies confirm PSMA expression in tumor-associated neovasculature. Cancer Res 1999;59(13):3192–3198; epub 1999/07/09.
29. Meighan MA, Dickerson MT, Glinskii O, Glinsky VV, Wright GL Jr, Deutscher SL. Recombinant glutamate carboxypeptidase II (prostate specific membrane antigen – PSMA) – cellular localization and bioactivity analyses. J Protein Chem 2003;22(4):317–326; epub 2003/09/19.
30. Carter RE, Feldman AR, Coyle JT. Prostate-specific membrane antigen is a hydrolase with substrate and pharmacologic characteristics of a neuropeptidase. Proc Natl Acad Sci USA 1996;93(2):749–753; epub 1996/01/23.
31. Smith-Jones PM, Vallabhajosula S, Navarro V, Bastidas D, Goldsmith SJ, Bander NH. Radiolabeled monoclonal antibodies specific to the extracellular domain of prostate-specific membrane antigen: preclinical studies in nude mice bearing LNCaP human prostate tumor. J Nucl Med 2003;44(4):610–617; epub 2003/04/08.
32. Wolf P, Freudenberg N, Buhler P, Alt K, Schultze-Seemann W, Wetterauer U, et al. Three conformational antibodies specific for different PSMA epitopes are promising diagnostic and therapeutic tools for prostate cancer. Prostate 2010;70(5):562–569; epub 2009/11/26.
33. Liu H, Moy P, Kim S, Xia Y, Rajasekaran A, Navarro V, et al. Monoclonal antibodies to the extracellular domain of prostate-specific membrane antigen also react with tumor vascular endothelium. Cancer Res 1997;57(17):3629–3634; epub 1997/09/01.
34. Li Y, Tian Z, Rizvi SM, Bander NH, Allen BJ. In vitro and preclinical targeted alpha therapy of human prostate cancer with Bi-213 labeled J591 antibody against the prostate specific membrane antigen. Prostate Cancer Prostat Dis 2002;5(1):36–46; epub 2004/06/15.
35. Holland JP, Divilov V, Bander NH, Smith-Jones PM, Larson SM, Lewis JS. 89Zr-DFO-J591 for immunoPET of prostate-specific membrane antigen expression in vivo. J Nucl Med 2010;51(8):1293–1300; epub 2010/07/28.
36. Pandit-Taskar N, O'Donoghue JA, Morris MJ, Wills EA, Schwartz LH, Gonen M, et al. Antibody mass escalation study in patients with castration-resistant prostate cancer using 111In-J591: lesion detectability and dosimetric projections for 90Y radioimmunotherapy. J Nucl Med 2008;49(7):1066–1074; epub 2008/06/17.
37. Roch A, Muller RN, Gillis P. Theory of proton relaxation induced by superparamagnetic particles. J Chem Phys 1999;110(11):5403–5411.
38. Forge D, Gossuin Y, Roch A, Laurent S, Elst LV, Muller RN. Development of magnetic chromatography to sort polydisperse nanoparticles in ferrofluids. Contrast Media Mol Imag 2010;5(3):126–132.
39. Serda RE, Adolphi NL, Bisoffi M, Sillerud LO. Targeting and cellular trafficking of magnetic nanoparticles for prostate cancer imaging. Mol Imaging 2007;6(4):277–288; epub 2007/08/23.
40. Mosmann T. Rapid colorimetric assay for cellular growth and survival: application to proliferation and cytotoxicity assays. J Immunol Methods 1983;65(1–2):55–63; epub 1983/12/16.
41. Bander NH, Milowsky MI, Nanus DM, Kostakoglu L, Vallabhajosula S, Goldsmith SJ. Phase I trial of 177lutetium-labeled J591, a monoclonal antibody to prostate-specific membrane antigen, in patients with androgen-independent prostate cancer. J Clin Oncol 2005;23 (21):4591–4601; epub 2005/04/20.
42. Rabin Y. Is intracellular hyperthermia superior to extracellular hyperthermia in the thermal sense? Int J Hyperthermia 2002;18 (3):194–202; epub 2002/05/25.
43. Haase C, Nowak U. Role of dipole–dipole interactions for hyperthermia heating of magnetic nanoparticle ensembles. Phys Rev B 2012;85 (4):045435.